Attenuation of low-frequency pressure fluctuations within the test section of an aeroacoustic wind tunnel using Helmholtz resonators

Alexander Bald[1], Kathrin Stahl[2], Holger Foysi[1], Sabine Roller[2]

[1] *Lehrstuhl für Strömungsmechanik, 57068 Siegen, Deutschland, Email: alexander.bald@uni-siegen.de*

[2] *Institut für Softwaremethoden zur Produkt-Virtualisierung, DLR, 01219 Dresden, Deutschland*

Abstract

A new aeroacoustic wind tunnel with an open test section was built at the University of Siegen. During the operation, infrasound tonal components and overtones reaching almost 110 dB in amplitude could be observed, sometimes influencing the measurements due to induced vibration of the wind tunnel structure. The present paper demonstrates the application of Helmholtz resonators on a pilot basis, which successfully attenuated these low-frequency peaks drastically. A systematic analysis using Helmholtz resonators with varying neck lengths was conducted. A single Helmholtz resonator, though able to tackle a target frequency, wasn't enough to get rid of other low-frequency components, leading to the use of two resonators. Additionally, the first application of the wind tunnel is shown to get an idea of its capabilities.

Wind Tunnel

The occurrence of wind tunnel low-frequency fluctuations within the open test section is a well-known phenomenon [10]. Flow instabilities due to small inhomogeneities, roughness effects, temperature fluctuations, or acoustic waves, for example, cause vortex shedding from the wind tunnel nozzle exit [10, 4]. Usually, this manifests itself in vortex ring structures propagating downstream and finally interacting with the collector and the tunnel diffuser, causing acoustic waves. As the open test section is enclosed within a semi-anechoic chamber (plenum chamber), different types of resonances are thus possible, which usually are described using simplified approaches. Therefore, the literature describes tube resonances within the tunnel duct, cavity resonances within the anechoic chamber or Helmholtz-type resonances if the collector or nozzle are seen as a resonator neck [10, 2]. The tube resonance is due to the coincidence of the shedding frequency with an acoustic resonance mode of the wind tunnel duct resulting finally in a standing wave in the duct. The resonance frequency f_R is thus calculated as

$$f_R = \frac{c}{2}\frac{m_R}{L_R}, \tag{1}$$

with speed of sound c, mode order $m_R \in \mathbb{N}$ and wind tunnel duct length L_R. The duct length was determined to be 33.6 m. The edgetone resonance frequency f_E describes the feedback loop between vortex-collector interaction, generating pressure waves traveling to the upstream end of the test section, and the nozzle lip, where vortex shedding is influenced [1]:

$$f_E = \frac{1}{L_{MS}}\left(\frac{1}{m_E R_{con} u} + \frac{1}{c-u}\right)^{-1}, \tag{2}$$

with fluid velocity u, mode $m_E \in \mathbb{N}$, mean convection rate $R_{con} \in [0.65, 0.7]$ and length of the test section L_{MS}.

Figure 1 depicts the new aeroacoustic wind tunnel at the University of Siegen. The maximum velocity is 70 m/s, the turbulence intensity level Tu_x varies between 0.14% and 0.28%, departures from velocity homogeneity are below 0.12 % and the temperature can be set within an uncertainty of ±1 K. For the measurements presented

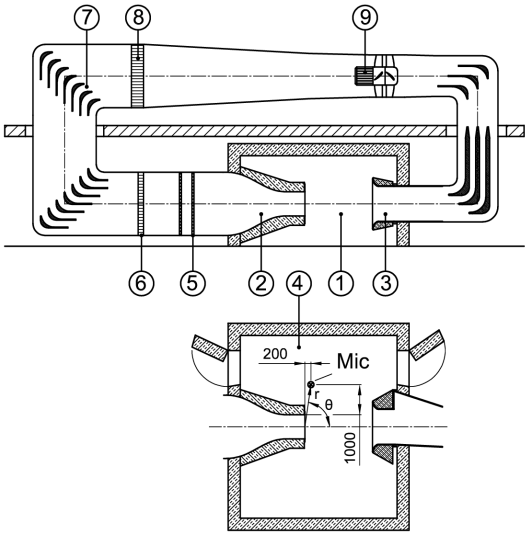

Figure 1: (1) Open test section; 0.8 m x 0.8 m x 2.24 m (2) Nozzle; area ratio 6.9 (3) Collector; 1.2 m x 1.2 m; can be moved horizontally (4) Plenum/semi-anechoic chamber 6.06 m x 5.2 m x 3.0 m (W x L x H) with sound-absorbing coating to provide acoustic semi-free-field conditions (5) Settling chamber with fences (6) Honeycomb rectifier (7) Deflection corners, built as splitter attenuators (8) Heat exchanger with cooling system (9) Fan; D = 1400 mm, ν=0.4 .

in this paper, the following measurement equipment was used

- 1/2" Free field microphone, type 4190-L-001 mounted on preamplifier type 2669 (Brüel & Kjær (B&K))
- NEXUS-amplifier/signal conditioner type 2690 (B&K)
- A/D-converter PXI-1033 (National instruments)

The microphone was positioned within the plenum chamber at a horizontal position (x,y) of (0.2m, 1m) after the nozzle exit edge. The A-weighted overall background sound pressure level (OASPL) for various velocities is shown in table 1. The corresponding SPL narrowband spectra (Δf = 1 Hz) are not shown due to brevity, here. In order to compare the present wind tunnel to equivalent facilities found in the literature, figure 2 shows the scaled overall sound pressure level OASPL_{scaled} (with indicated microphone position) as a function of velocity defined as:

$$\mathrm{OASPL}_{scaled} = \mathrm{OASPL}_{fac} - 10\log_{10}(A_{fac}/r_{fac}^2), \tag{3}$$

with overall sound pressure level of the facility OASPL_{fac}, nozzle exit area A_{fac} and distance of microphone to center nozzle exit r_{fac} (see figure 1) [11, 8, 6, 3]. It can be seen, that the wind tunnel exhibits excellent noise levels when compared to other facilities.

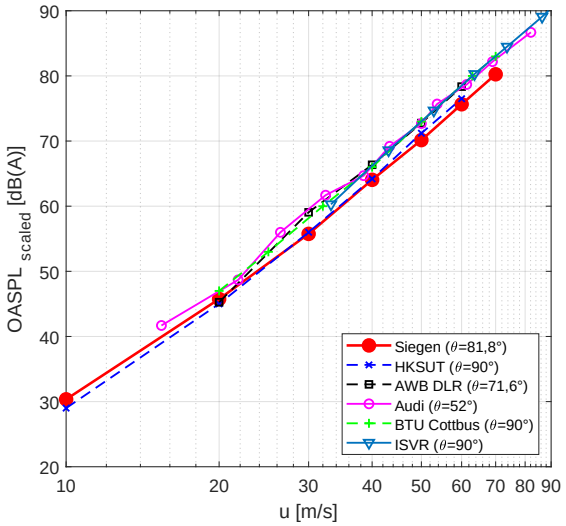

Figure 2: Comparison of selected wind tunnels to the new tunnel built in Siegen. For definition of θ see figure 1. Data from [11, 8, 6, 3].

Low-frequency pressure fluctuations

During the measurement campaigns, strong low-frequency pressure fluctuations were observed. The measured spectra showed large peaks at specific frequencies, as illustrated exemplarily in figure 3, showing a narrowband spectrum at $u = 24$ m/s. The depicted large peaks can be seen to reach 104 dB, exceeding the background by over 30 dB. The fluctuations were sometimes able to excite even vibrations in the wind tunnel structure. In order to quantify these peaks further, figure 4 summarizes the maximum amplitude of these frequencies as a function of the wind tunnel velocity (blue). The bands at 9 Hz and 18 Hz are clearly strongest, reaching 108 dB. From approximately 28 m/s to 40 m/s, no significant low-frequency peaks were observed in the spectra. Various investigations in the past link these peaks to resonances due to standing waves, plenum modes or edgetone modes [1, 10, 5]. Figure 5 therefore shows the frequency of the various SPL peaks measured for different wind tunnel velocities. Four bands are recognized, located at 9 Hz, 12 Hz, 18 Hz and 24 Hz. Superimposed on this data, the resonance frequencies according to standing wave modes calculated via the expression in (1) and the edgetone resonance frequency from (2) can be seen. All bands except the 24 Hz band agree well with the standing wave modes and nicely align with the $m_R = 2$ to $m_R = 4$

Table 1: A-weighted overall sound pressure level (OASPL), calculated using the third-octave bands from 50 Hz to 20 kHz.

u [m/s]	0	10	20	30
OASPL [dB(A)]	22	25	41	51
u [m/s]	40	50	60	70
OASPL [dB(A)]	59	65	71	75

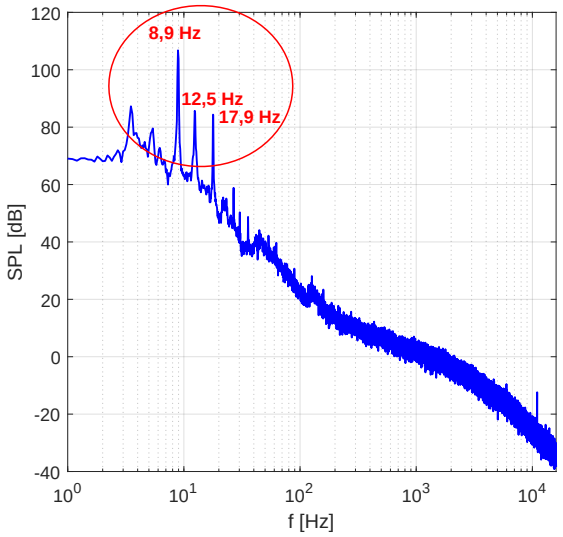

Figure 3: SPL narrowband spectrum ($\Delta f = 0.1$Hz), demonstrating low-frequency peaks in the test section at $u = 24$m/s.

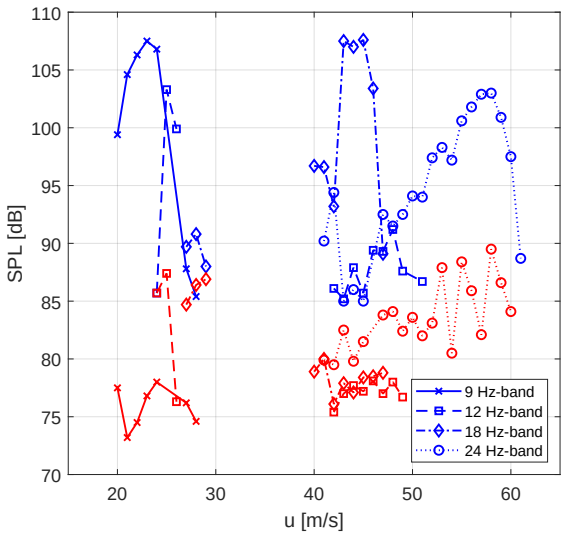

Figure 4: Peak SPL of the pressure fluctuations as a function of the wind tunnel velocity before (blue) and after (red) using Helmholtz resonators.

modes. Interestingly, the 12 Hz and 24 Hz bands seem to imply resonance with edgetone feedback, too. The first and second edgetone modes seem to resonate with the 12 Hz band at higher and lower velocities, respectively. Although Ahuja *et al.* [1] considered the edgetone modes to be important for Mach number larger than 0.3, only, we cannot rule out the edgtone feedback to influence and amplify the standing wave mode $m_R = 2$ for this frequency band. Jin *et al.* [5] observed edgetones in their investigated low Mach wind tunnel, too, although in this case cavity resonance was excited by the edgetone resonance. The 24 Hz band resonance frequency does not align with the standing wave modes, instead, we see a clear continuous progression with increasing velocity from the $m_R = 5$ to the $m_r = 6$ resonance mode, in addition to the 2nd edgetone mode showing a good qualitative agreement with the measured data. Speculation so far is that the 2nd edgetone mode is causing this band's resonance frequency transition between the two standing wave modes, this is under current investigation.

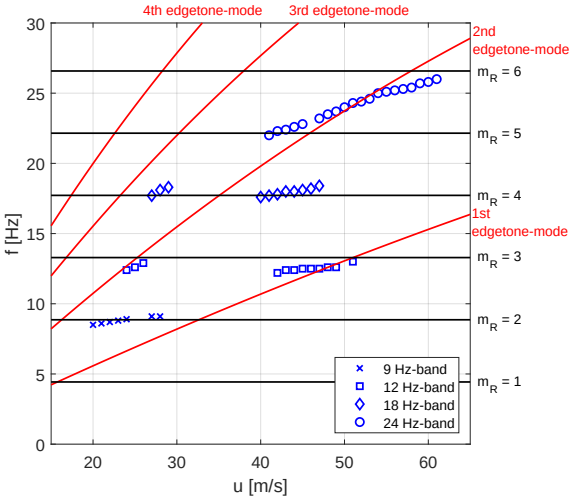

Figure 5: Low-frequency pressure fluctuations compared to edgetone and standing wave modes (equations (2) and (1)).

Helmholtz-Resonator

In order to attenuate the observed fluctuations, Helmholtz resonators were built and attached to the wind tunnel. Measurements were done using a single Helmholtz resonator in a first step, in order to attenuate higher frequency components in addition, a second resonator was used as described below, too. Figure 6 shows the resonators with variable neck lengths and indicates the position within the wind tunnel technical drawing. The resonator frequency of the Helmholtz resonator is

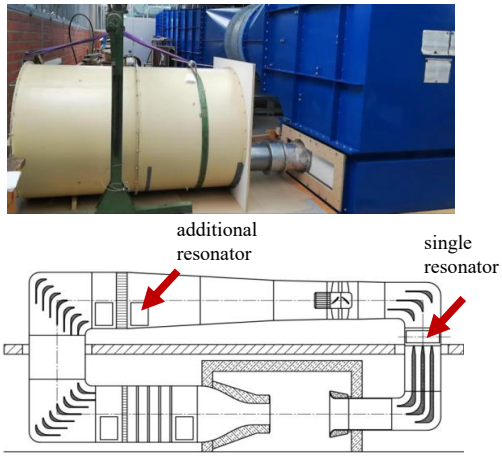

Figure 6: Position of Helmholtz resonators with variable neck (top) at maintenance opening, indicated by the red arrows (bottom image).

given as

$$f_0 = \frac{c}{2\pi}\sqrt{S/(VL_{eff})}, \qquad L_{eff} = L + 2\Delta L, \quad (4)$$

with L_{eff} being the effective neck length, L the real neck length, the end correction of the neck length ΔL and resonator volume V. Different expressions can be found in the literature for ΔL, with $\Delta L \in [\pi r/4\ ,\ \Delta L = 8r/3\pi]$ and neck radius r [9, 2]. A systematic investigation using more than 1000 measurements to determine the optimum neck length with maximum attenuation at various velocities was conducted. Figure 7 shows an example for $u = 43$ m/s. Attenuation of the peaks for optimal neck length of up to $\Delta L_p \approx 24$ dB was possible with one Helmholtz resonator, reducing the main peak to values smaller than $L_p = 85$ dB (blue curve). Furthermore, overtone components could be influenced and damped, too. However, damping only occurred within one frequency band, peaks in other bands were even sometimes increasing, as can be seen in the 24 Hz peak, which was increasing clearly. Therefore, 2 Helmholtz resonators were used, with the second tackling other dominant frequencies. This resulted in dampening all the major fluctuations successfully (red curve)! The effect of the resonators on the peak SPL of the low-frequency pressure fluctuation is summarized in figure 4 (red) above, demonstrating the successful attenuation making those fluctuations unproblematic for future measurement campaigns. Investigations using external and internal necks showed no significant difference. Therefore, internal necks will be used in the future due to easier handling during measurements.

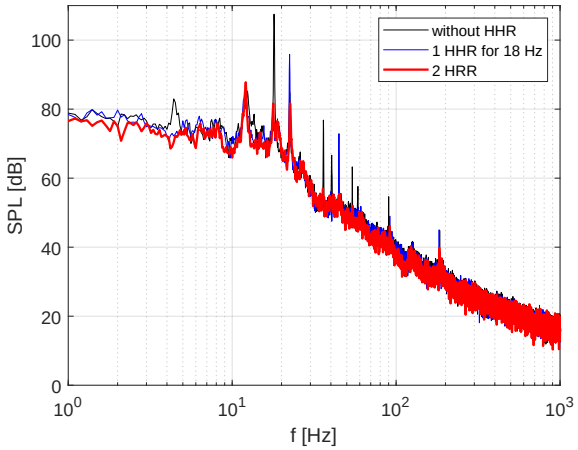

Figure 7: SPL for $u = 43$ m/s comparing the situation without (black line), one (blue line), and two Helmholtz resonators (red line).

Application example: Blunt trailing edge noise of a cambered airfoil

The wind tunnel was utilized in an initial project to investigate blunt trailing edge noise (BTEN) of cambered airfoils for different chord-based Reynolds numbers Re_c under different aerodynamic loads which were realized in varying the effective angles of attack (AoA) α_e. The airfoil selected was a DU93W210, vertically mounted as depicted in figure 8. An exchangeable trailing edge section allowed the application of sections with different trailing edge thickness-to-chord ratios t^*. Wherein t^* represents

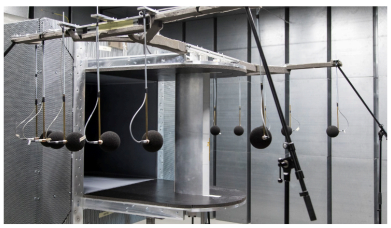

Figure 8: Experimental setup for the BTEN study with DU93W210 airfoil section. The microphones are placed at a distance of $3.3c_b$ (c_b refers to the chord length of the unmodified airfoil with $t^* = 0.005$) and rotate with the AoA, thereby keeping their relative positions.

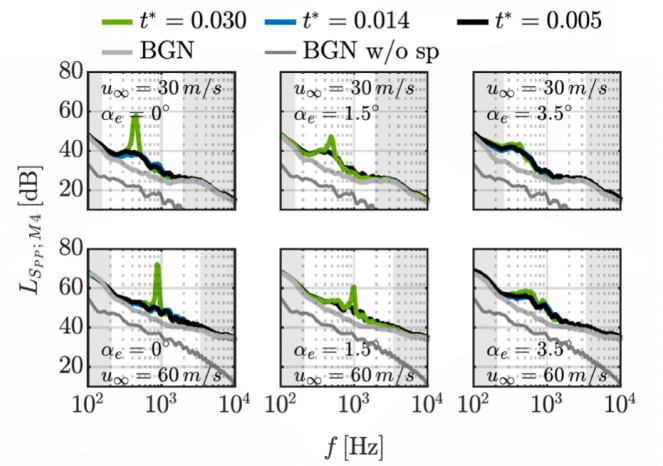

Figure 9: PSD of the far-field noise for different velocities, AoA α_e and trailing edge thickness-to-chord ratios t^*.

the ratio of the trailing edge thickness t_{TE} to the chord length c. This installation allowed capturing the deflected air stream optimally, using a horizontally movable collector, this way minimizing noise by the air stream hitting the collector. The side plates, through which the airfoil is attached, are lined with 2 cm thick acoustic foam to absorb noise. To adjust the AoA, the airfoil can be rotated vertically. Figure 9 presents a small excerpt from the results of the study with the spectral power density (PSD) of the far-field noise of the investigated configurations (variation of t^*, AoA, and Re_c). Additionally, the background noise with (BGN) and without side plates (BGN w/o sp) is shown. Areas with insufficient signal-to-noise ratio are grayed out. Within the frequency range of interest (BTEN peaks), there is a sufficiently large signal-to-noise ratio and the characteristics of the different configurations can be accurately compared. Finally, a comparison of the measured surface pressure fluctuations Φ_{pp} on the suction side at $x/c = 0.93$ position for $t^* = 0.005$, 0° effective AoA and u_∞=60 m/s to LBM simulations using PowerFlow [7] is shown in figure 10, indicating very good agreement between simulation and experiment. The f^{-2} decay is similar to that observed in [12] and others cited therein. In addition to the measurement of the far-field noise, surface pressure fluctuations on suction and pressure sides, the pressure distribution of the airfoil, and extensive flow field measurements using hot-wire anemometry were also carried out in this exemplary study. The results will be published separately.

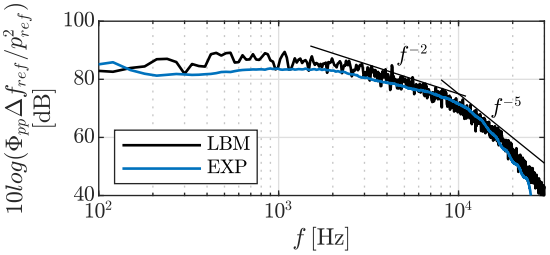

Figure 10: PSD of surface pressure fluctuations Φ_{pp} on the suction side at $x/c = 0.93$ compared to LBM simulations using PowerFlow [7]. The reference frequency band is Δf_{ref} = 30 Hz, the reference pressure $p_{ref} = 2 \times 10^5$ Pa, the sample frequencies $f_{S,EXP}$ = 51.2 kHz and $f_{S,LBM}$ = 10 MHz.

Conclusion

An aeroacoustic wind tunnel with an open test section was built. Low-frequency pressure fluctuations were observed at various velocities, coinciding with standing wave tube resonances modes (eq. (1)). The 12 Hz and 24 Hz bands seem to be generated in addition by resonance of the tube modes with edgetone feedback, since agreeing with edgetone frequencies, too, despite those usually reported to be important for higher Mach number flows, only [1]. Further research is required and is planned in addition to a practical implementation of the resonators for future work. Finally, the capability of the wind tunnel to investigate state-of-the-art problems was demonstrated.

Acknowledgment

The authors thank the Deutsche Forschungsgemeinschaft (DFG) for support (INST 221/97-1 FUGG) and Ayman Haidar for his work during his bachelor thesis.

References

[1] Ahuja, K., Massey, K., and D'Agostino, M. *Flow/acoustic interactions in open-jet wind tunnels*, vol. AIAA 1997-1691. 1997.

[2] Barron, R. F. *Industrial Noise Control and Acoustics*. Crc Press Inc, 2002.

[3] Chong, T., Joseph, P., and Davies, P. Design and performance of an open jet wind tunnel for aeroacoustic measurement. *Appl. Acoust. 70* (2009), 605.

[4] Foysi, H., Mellado, M., and Sarkar, S. Simulation and comparison of variable density round and plane jets. *Int. J. Heat & Fluid Flow 31* (2010), 307.

[5] Jin, L., Deng, X. B., Wang, X., Gu, Y., Liang, Y., and Lian, Z. Standing waves in the plenum of an open jet wind tunnel: Resonance and self-excited oscillation. *AIP Advances 12*, 2 (2022), 025105.

[6] Pott-Pollenske, M., and Delfs, J. Enhanced capabilities of the aeroacoustic wind tunnel braunschweig. *AIAA 2008-2910* (2008).

[7] Powerflow. *https://www.3ds.com/de/produkte-und-services/simulia/produkte/powerflow/*.

[8] Sarradj, E., Fritzsche, C., Geyer, T., and Giesler, J. Acoustic and aerodynamic design and characterization of a small-scale aeroacoustic wind tunnel. *Applied Acoustics 70* (2009), 1073–1080.

[9] Selamet, A., Radavich, P. M., D. N., and Novak, N. Circular concentric helmholtz resonators. *J. Acoust. Soc. Am. 101*, 1 (1997), 41–51.

[10] Wickern, G., von Heesen, W., and Wallmann, S. Wind tunnel pulsations and their active suppression. *SAE Transactions 109* (2000), 1403.

[11] Yi, W., Zhou, P., Fang, Y., Guo, J., Zhong, S., Zhang, X., H. X., Zhou, G., and Chen, B. Design and characterization of a multifunctional low-speed anechoic wind tunnel at HKUST. *Aerospace Sci. Technology 115* (2021), 106814.

[12] Zang, B., Mayer, Y., and Azarpeyvand, M. Experimental investigation of near-field aeroacoustic characteristics of a pre- and post-stall naca 65-410 airfoil. *J. of Aerospace Engineering 34*, 6 (2021).